Journal of
Mechanics of
Materials and Structures

EFFECT OF INTERCONNECT LINEWIDTH ON THE EVOLUTION OF
INTRAGRANULAR MICROCRACKS DUE TO SURFACE DIFFUSION IN A
GRADIENT STRESS FIELD AND AN ELECTRIC FIELD

Linyong Zhou, Peizhen Huang and Qiang Cheng

msp

EFFECT OF INTERCONNECT LINEWIDTH ON THE EVOLUTION OF INTRAGRANULAR MICROCRACKS DUE TO SURFACE DIFFUSION IN A GRADIENT STRESS FIELD AND AN ELECTRIC FIELD

LINYONG ZHOU, PEIZHEN HUANG AND QIANG CHENG

Based on the weak formulation for combined surface diffusion and evaporation/condensation, we derive the governing equation of the finite-element induced both by stressmigration and electromigration. The corresponding program is developed for simulating the evolution of the intragranular microcracks caused by surface diffusion in copper interconnect lines under a gradient stress field and an electric field. Unlike previously published works, this paper is focused on how the interconnect linewidth influences the microcrack evolution. Numerical analysis results show that there exists a critical value of the linewidth $\hat{h}_c$. When $\hat{h} > \hat{h}_c$, the microcrack will drift along the direction of the electric field by a stable form. When $\hat{h} \leq \hat{h}_c$, it will split into two small microcracks and the decrease of the linewidth is beneficial for the microcrack splitting. Besides, the critical linewidth increases with the increase of the electric field and the aspect ratio, and the critical linewidth first increases and then decreases with the increase of the stress gradient. That is, the increase of the electric field and the aspect ratio is beneficial for the microcrack to split. In addition, all of the critical values of the electric field, the aspect ratio and the stress gradient decrease with the decrease of the linewidth. The microcrack has a stronger dependence on the linewidth when $\hat{h} < 25$.

1. Introduction

Interconnect lines are widely used in micro-devices. With the trend of miniaturization and integration of microelectronic systems, the feature size on the integrated circuit chip continues to decrease, following the sharp increase in current density and the sharp decrease in interconnect linewidth. Interconnect lines are usually subjected to severe mechanical and electrical load [Bower and Craft 1998]. In addition, interconnect lines inevitably exist some drawbacks, such as voids and microcracks. If the voids or microcracks grow and change their shape, they could affect the reliability of interconnects [Bower and Shankar 2007]. Therefore, it is significant to understand the effect of linewidth on the evolution of microcracks in a stress field and an electric field [Krug and Dobbs 1994; Schimschak and Krug 1997].

Over the last forty years, the behavior of electromigration and stressmigration has been studied extensively because it can seriously affect the reliability of the conductor lines. Due to the technological need in microelectronic industry, measurement (see [Cho and Thompson 1989; Dreyer and Varker 1992], for instance) and prediction of time-to-failures (see [Bower and Craft 1998; Giroux et al. 1995; Zhang et al. 2010], for example) and their distributions have dominated electromigration testing and modelling in the past. And the mass transport mainly occurs through interfacial diffusion and grain boundary diffusion.

The results also indicate that growth, drift, and accumulation of existing voids lead to the observed strong linewidth dependence. Furthermore, in situ observations of the damage development have shown that failure of interconnect lines is a complicated process including nucleation, growth, motion and shape changes of voids [Vairagar et al. 2004]. There are some voids within a grain [Kraft et al. 1993] except on a grain boundary. The evolution of voids within a grain changes its shape only through surface diffusion. And the morphology of voids within a grain due to surface diffusion induced by electromigration or by stressmigration has been investigated in detail.

There have been a number of analytical studies on the electromigration-induced void morphological evolution under high current density [Wang and Yao 2017a; 2017b], on predicting finger-shaped void propagation speed in solder interconnects [Yao et al. 2009], and on the steady motion velocity of an elliptical inclusion and voids under electromigration and a gradient stress field [Dong and Li 2009; Li et al. 2010]. In addition, Gungor and Maroudas [1999] showed a theoretical analysis for electromigration-induced failure of metallic interconnect lines and predicted that prevention of failure is possible by adjusting the grain orientation with respect to the applied electric field.

Experimental studies have revealed that the current density, the stress field and the self-diffusion coefficient can significantly affect the failure mechanism of the interconnect lines [Huntington and Grone 1961; Black 1969; Blech and Herring 1976; Blech 1998; Zschech et al. 2010; Vanstreels et al. 2014; Lin et al. 2017]. In addition, when the electric current passing through the interconnect lines, the metal atoms flow out from the cathode of the interconnect line into the anode induced by electromigration. And they deposit at the anode, forming a linear gradient stress field [Dong and Li 2009]. The gradient stress, in its turn, motivates atoms to diffuse on the microcrack surface, changing its shape and position. This coupling effect has never been quantitatively analyzed.

There are also many numerical analyses on stressmigration and electromigration due to diffusion processes [Bower and Craft 1998; Bower and Shankar 2007; Bower and Freund 1993; Kraft and Arzt 1995; Sun and Suo 1997; Sun et al. 1997; Xia et al. 1997; Liu et al. 1998; Dalleau and Weide-Zaage 2001; Fridline and Bower 2002; Liu and Yu 2006]. Several authors [Bower and Craft 1998; Bower and Freund 1993; Xia et al. 1997; Kraft and Arzt 1995] showed two dimensional finite-element simulations of void evolution due to strain and electromigration induced surface diffusion. They discussed the failure mechanisms and the nucleation, growth and evolution of voids in the interconnect lines of microelectronic circuits, including the effect of linewidth on the failure time. Before long, the method was extended to three-dimensional problems [Zhang et al. 1998]. Electromigration induced void nucleation, growth and evolution have been extensively studied by the finite-element method [Dwyer 2010]. The failure analysis of critical-length data from electromigraion was studied [Dwyer 2011], which is corresponding to the experiment results [Blech 1998]. The numerical method mentioned above is on the weak formulation including curvature, electric field and stress field [Bower and Shankar 2007; Xia et al. 1997; Fridline and Bower 1999]. But the finite-element method combined surface diffusion and evaporation/condensation was first built in [Sun and Suo 1997], which has since been applied to a range of problems, such as grain growth [Huang et al. 2003b], faceted crystals and grain boundary grooving [Liu and Yu 2006], the evolution of a bicrystal film and a tricrystal film on a substate, and the morphological evolution of microcracks [Huang et al. 2003a; 2003c; Huang and Sun 2004; Wang et al. 2006]. In recent years, the finite-element method based on the weak formulation combined surface diffusion and evaporation/condensation has

been extended and applied to studied the microcrack evolution caused by surface diffusion induced by stressmigration [He and Huang 2014] and electromigration [He and Huang 2015].

However, the weak formulation incorporating surface diffusion and evaporation/condensation induced both by electromigration and stressmigration has not been reported in the literature up to now. And no report has analyzed the effect of interconnect linewidth on the morphological evolution of intragranular microcrcacks due to surface diffusion in a gradient stress field and an electric field. The aim of the present work reported here is primarily to develop a finite-element program to simulate the morphological evolution of the intragranular microcracks under a gradient stress field and an electric field. And the work is focused on how the interconnect linewidth influences the microcrack evolution.

This paper is organized as follows. In Section 2, we introduce our analysis model of two-dimensional intragranular microcrack, then briefly describe the basic diffusion theory and develop the finite-element method induced both by stressmigration and electromigration in Section 3. In Section 4, the microcrack evolution is simulated under different linewidths, gradient stress fields, electric fields and aspect ratios, and the corresponding effect is discussed. Section 5 presents the main conclusion.

2. Modeling of two-dimensional intragranular microcrack evolution

Interconnect lines are usually under large stress. The stress in an interconnect line arises mainly from two sources: heat and electromigration. Current passes through the interconnect line, causing atoms to migrate in the direction of electron flow. The matter transports on the microcrack surface and it causes the shape change and the motion of the microcrack. The electromigration causes atoms depletion near the cathode and deposition near the anode of the line. It leads to a gradient stress along the interconnect line with a tensile stress near the cathode and compressive stress near the anode as shown in Figure 1. The gradient stress, in its turn, motivates atoms to diffuse on the microcrack surface, changing its shape and position.

Figure 2 shows the model of our analysis. The interconnect line is idealized as a two-dimensional single crystal with a microcrack along the midline and is assumed in a state of plain strain. The line is subjected to an electric field as a voltage V_0 and a linear gradient stress filed with a tensile stress near the cathode and compressive stress near the anode which is induced in the interface between the line and the passivation. We assume that the distribution of the voltage in the boundary is uniform and that
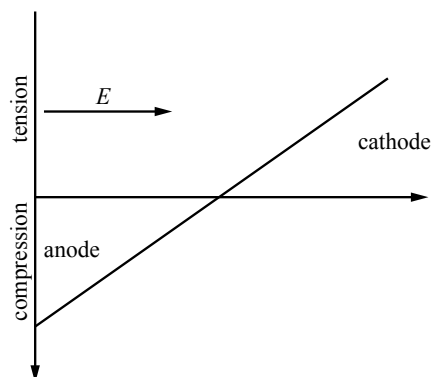
Figure 1. Schematic illustration of the gradient stress induced by electromigration.
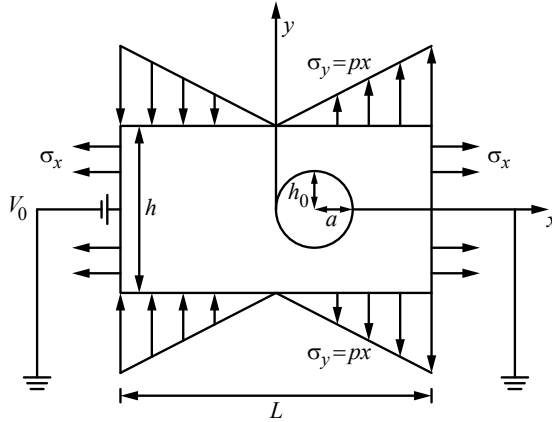
Figure 2. A model of an intragranular microcrack under a gradient stress field and an electric field.

the electric field in the line has no component normal to the plane of the figure. Diffusion through the bulk is assumed to be negligible. Therefore, in the absence of grain boundaries, the only mode of mass transport is diffusion along the microcrack surface. We have assumed that the surface energy is isotropic and that the surface energy does not interfere with the electric field energy and the strain energy.

For simplicity, the microcrack is characterized by the aspect ratio $\beta = a/h_0$, where a is the initial major semiaxis of the microcrack, h_0 is the initial minor semiaxis, L is the length of the interconnect line, and h is the linewidth.

3. Basic theory

3.1. *Surface diffusion equations.* Based on Herring's classical theory [Herring 1999], we adopt a kinetic law that, at every point on the grain surface, the flux of the surface diffusion, J, is proportional to the driving force F:

$$J = MF. \tag{1}$$

Here M is the mobility of atoms on the surface; it is related to the self-diffusivity by the Einstein relation, $M = \Omega D\delta/kT$, in which Ω is the volume of the atom, D is the self-diffusivity on the surface, δ is the effective thickness of atoms participating in matter transport, k is Boltzmann's constant, and T is the absolute temperature. The driving force F is defined by the decrease in free energy per unit volume of matter moving per unit distance on the surface.

As matter is deposited onto or removed from a free surface, a normal velocity v_{ns} of the free surface results. Mass conservation requires that

$$v_{ns} = -\nabla \cdot J, \tag{2}$$

where $\nabla \cdot J$ is the surface divergence of the flux vector. Let δr_{ns} be the virtual normal displacement on the surface and δI be the virtual mass displacement; we have

$$\delta r_{ns} = -\nabla \cdot \delta(I). \tag{3}$$

Given a microcrack, the driving force, $\boldsymbol{F}$, according to the kinetic law, drives the flux $\boldsymbol{J}$ to conserve the microcrack mass, the divergence of the flux gives rise to the surface velocity, which then updates the shape for a small time increment. Repeat the procedure for many time increments to trace the evolving microcrack shape. However, a surface diffusion problem that conserves solid mass as formulated above is difficult to implement in a finite-element setting. Once an evaporation/condensation process is introduced into microstructure evolution, the overall mass conservation is easier to treat by a finite-element method [Sun and Suo 1997].

3.2. Weak statement for combined surface diffusion and evaporation/condensation. Following the principle of virtual work [Sun et al. 1994], we obtain the integral form

$$\int \boldsymbol{F} \cdot \delta \boldsymbol{I} \, dA = -\delta G, \tag{4}$$

where δG is the increment in free energy and dA is the area of the element. Substituting (1) into (4), we have

$$\int \frac{\boldsymbol{J} \cdot \delta \boldsymbol{I}}{M} \, dA = -\delta G. \tag{5}$$

Once $\boldsymbol{J}$ is solved from (5), the surface normal velocity is obtained from (2), which then updates the shape for a small increment.

Imagine two concurrent processes on a microcrack surface: surface diffusion and evaporation/condensation. The kinetic law for evaporation/condensation is similar to the surface diffusion. Let p be the free energy reduction associated with per unit volume of matter added to per unit surface area of the microcrack, and v_{nv} be the volume of matter added to per unit area of the microcrack surface per unit time. They are proportional to each other:

$$v_{nv} = mp, \tag{6}$$

where m is the mobility of evaporation/condensation. The resulting equations of the surface normal velocity v_n and the surface virtual displacement δr_n due to the combined action of evaporation/condensation and surface diffusion are

$$v_n = v_{nv} - \nabla \cdot \boldsymbol{J}, \tag{7}$$

$$\delta r_n = \delta r_{nv} - \nabla \cdot \delta \boldsymbol{I}. \tag{8}$$

Associated with the virtual motion, the free energy changes by δG. According to the two kinds of driving forces, $\boldsymbol{F}$ and p, matter relocation and exchange on the microcrack surface area element, δA, reduce the free energy by $(\boldsymbol{F} \cdot \delta \boldsymbol{I} + p \delta r_{nv}) dA$. Thus, we have the weak formulation for combined surface diffusion and evaporation/condensation:

$$\int (\boldsymbol{F} \cdot \delta \boldsymbol{I} + p \delta r_{nv}) dA = -\delta G. \tag{9}$$

Substituting Equations (1)–(8) into (9), we have

$$\int \left(\frac{\boldsymbol{J} \cdot \delta \boldsymbol{I}}{M} + \frac{(v_n + \nabla \cdot \boldsymbol{J})(\delta r_n + \nabla \cdot \delta \boldsymbol{I})}{m} \right) ds = -\delta G. \tag{10}$$

The finite-element method introduced in [Sun and Suo 1997] is used for solving the above the weak formulation. The difference between references [Sun and Suo 1997; He and Huang 2014; He and Huang 2015] and this paper is that we consider the coupling with a gradient stress field and an electric field. The kinetic and mass conservation laws expressed in the left-hand side of (10) are the same, but the energy term in the right-hand side of (10) has two extra terms, the strain energy and the electric potential.

3.3. *Finite-element method.* The system consists of two coupled subsystems: the microcrack surface and the solid body (as shown in Figure 2). The motion of the microcrack surface is affected by the strain energy and the electric potential within the solid body, which in turn is affected by the shape changes due to the surface motion. Each subsystem is discretized into finite elements as follow. Following [Sun et al. 1997], we represent the microcrack surface by a set of linear isoparametric finite elements. Each element has four degrees of freedom to describe motion and three degrees of freedom to describe diffusion. These coordinates, together with mass displacement I at all the nodal points, form generalized coordinates

$$q_1, q_2, q_3, \ldots, q_{n-2}, q_{n-1}, q_n,$$

where n is the total number of degrees of freedom. The generalized velocities are

$$\dot{q}_1, \dot{q}_2, \dot{q}_3, \ldots, \dot{q}_{n-2}, \dot{q}_{n-1}, \dot{q}_n,$$

The velocity and virtual motion of any point on the surface can be interpolated by the corresponding values at the nodes. Integrating the weak statement equation (10) element by element, we get a bilinear form in $\dot{q}$ and δq. The right-hand side of (10) is the total free energy change associated with the virtual motion,

$$\delta G = - \sum f_i \delta q_i, \tag{11}$$

which allows us to compute the generalized forces $f_1, f_2, \ldots, f_n$. Collect the coefficient of δq_i, giving

$$\sum_j H_{ij} \cdot q_j = f_i. \tag{12}$$

The matrix H is symmetric and positive-definite, and both H and the force vector f depend on the coordinates of all the nodes. Equation (12) is a set of nonlinear ordinary differential equations and is solved by using the Runge–Kutta method. In this paper, for the sample problem to be simulated as shown in Figure 2, we consider surface energy, strain energy and electric potential. The free energy variation associated with a given element is computed as follows:

$$\delta G = \gamma_s \delta l - \int \omega \delta r_n + \frac{Z^* |e|}{\Omega} \int V \delta r_n \, ds, \tag{13}$$

where ω represents the strain energy density, γ_s is the element surface tension, Z^* is a phenomenological constant known as the effective valence of an atom, e is the charge of the electron and V is the electric potential. This is different from previous works for combining strain energy density and electric potential [He and Huang 2014; 2015]: the force components acting on the two nodes of the element due to the

element surface energy, strain energy and electric potential are

$$
\boldsymbol{f}^e = \gamma_s
\begin{bmatrix}
\cos\theta \\
\sin\theta \\
0 \\
-\cos\theta \\
-\sin\theta \\
0 \\
0
\end{bmatrix}
- \frac{l}{2}
\begin{bmatrix}
\left(\frac{2}{3}\omega_1 + \frac{1}{3}\omega_2\right)\sin\theta \\
-\left(\frac{2}{3}\omega_1 + \frac{1}{3}\omega_2\right)\cos\theta \\
0 \\
\left(\frac{1}{3}\omega_1 + \frac{2}{3}\omega_2\right)\sin\theta \\
-\left(\frac{1}{3}\omega_1 + \frac{2}{3}\omega_2\right)\cos\theta \\
0 \\
0
\end{bmatrix}
+ \frac{Z^*|e|l}{2\Omega}
\begin{bmatrix}
\left(\frac{2}{3}V_1 + \frac{1}{3}V_2\right)\sin\theta \\
-\left(\frac{2}{3}V_1 + \frac{1}{3}V_2\right)\cos\theta \\
0 \\
\left(\frac{1}{3}V_1 + \frac{2}{3}V_2\right)\sin\theta \\
-\left(\frac{1}{3}V_1 + \frac{2}{3}V_2\right)\cos\theta \\
0 \\
0
\end{bmatrix}.
$$

Here ω_1 and ω_2 represent the strain energy density of nodes 1 and 2, and V_1 and V_2 are the nodal values of the electric potential function.

Both the strain energy density and the electric potential on the microcrack surface affect the surface motion. We choose to discretize the solid body and use the standard finite procedure.

For each time step Δt, the calculations proceed as follows:

(i) Solve the electric field and the stress field problem on the current configuration, including the computation of the strain energy density, the electric potential and project the results onto the surface nodes.

(ii) Compute the new surface configuration.

(iii) Update the time.

4. Numerical simulation and discussion

In this section, based on the finite-element method for large change of a solid due to matter diffusion, the behavior of the intragranular microcracks caused by surface diffusion induced both by stressmigration and electromigration is analyzed by the finite-element method developed in this paper. We focus on how the interconnect linewidth influences the microcrack evolution. The reliability of the finite-element method under electric field has been conformed as shown in [He and Huang 2015]. Meanwhile, mass conservation requires that the total area of the microcrack remain constant. The actual change of this area during simulation can therefore be taken as a measure of the computing accuracy. We monitor the total area of a microcrack as a means to verify the accuracy of our numerical results. Large numbers of numerical calculations indicate that the finite-element method used is robust, accurate and efficient. For convenience, we introduce the dimensionless linewidth $\hat{h} = h : h_0$ to reflect the influence of the interconnect linewidth on the evolution of intragranular microcrack through changing the value of h. Additionally, we introduce the nondimensional time $\hat{t} = tM\gamma_s/h_0^4$ and a dimensionless stress gradient $\hat{p} = pLH_0/\gamma_s$. The relative magnitude of the two forces, the electromigration driving force and the surface tension, is given by $\chi = V_0|e|Z^*h_0/\Omega\gamma_s L$.

Figure 3 shows the evolution of intragranular microcracks for $\chi = 0.6$, $\beta = 4$, $\hat{p} = 29$ as the linewidth decreases ($\hat{h} = 80, 50, 20, 15$). As shown in each of the plots, the initial shape of the microcrack is elliptical and the curvature of each point on the microcrack surface is different. The pronounced difference in curvature along the microcrack perimeter induces mass redistribution, with mass being removed from relatively flat microcrack surfaces and depositing in the microcrack tips. From the initial stress
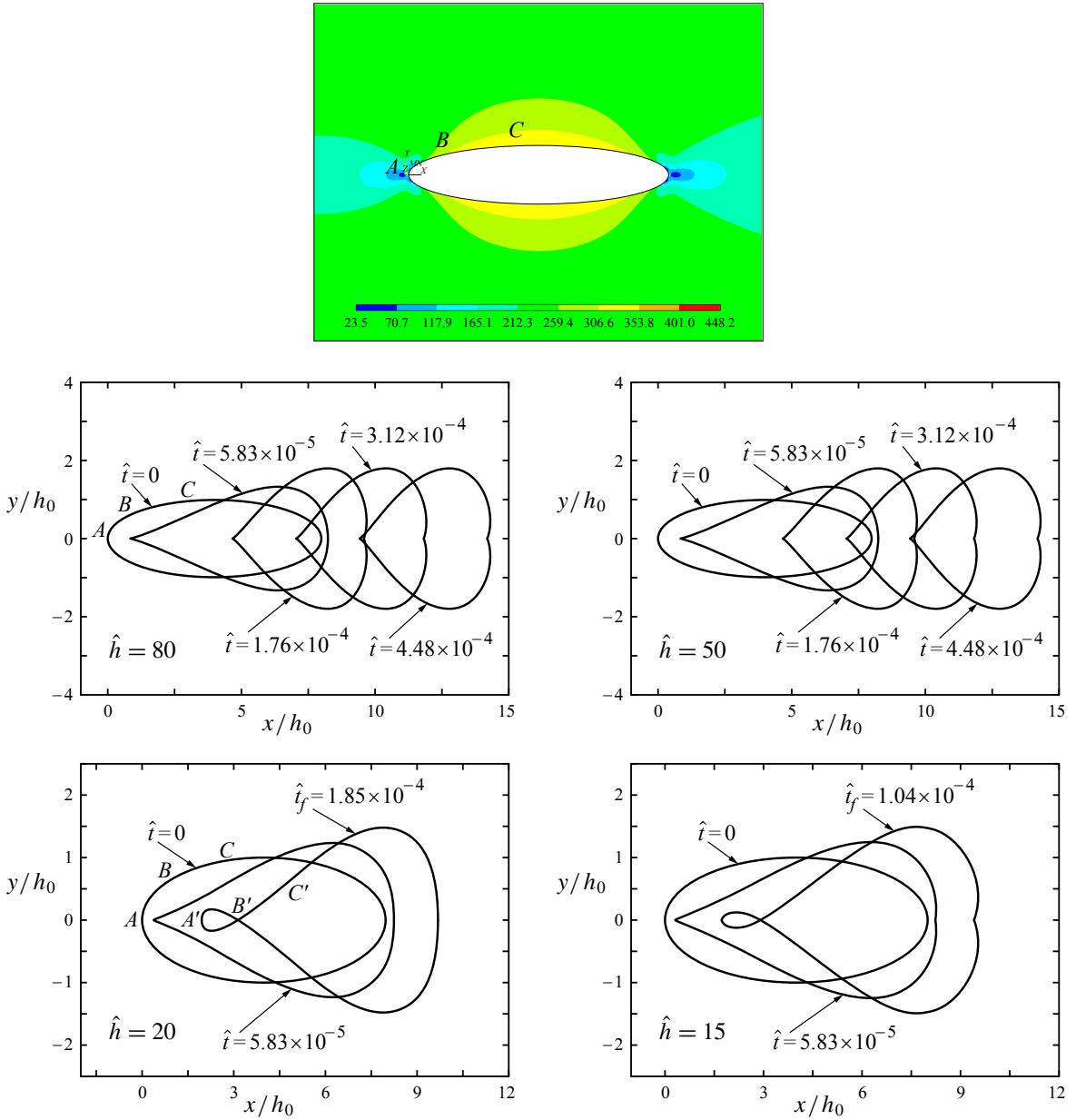
Figure 3. Initial stress nephogram (top; scale values in MPa) and evolution of the intra-granular microcrack for $\chi = 0.6$, $\beta = 4$, $\hat{p} = 29$. Note the different scales between graphs. Four values of $\hat{h}$ are illustrated: 80, 50, 20, 15.

nephogram (Figure 3, top) we see that $\omega_C > \omega_B > \omega_A$, which indicates that atoms in point C would move to point B and point A under the surface diffusion driving force induced by strain energy. Meanwhile, as we know, the electromigration driving force is proportional to the gradient of the electric potential. In the first time plot (middle row, left), we have $(\partial V/\partial s)_C > (\partial V/\partial s)_B > (\partial V/\partial s)_A$ at the initial time. So, the atoms in point C would move to point B, and then from point B to point A under the electromigration

driving force. If the stress field and electric field dominate the microcrack evolution, atoms deposited on point B start to form a bulge at the microcrack surface (seen as a shallow concavity on each side of the tip of the drop-shaped curve). With an increase in the gradient stress field and electric field, atoms continue to gather there.

With a decrease in linewidth, the current density increases and the stress gradient increases sharply. The bulges on the upper and lower surfaces can connect (point B' in bottom right panel), and then the cavity splits into two small microcracks, as shown in the bottom row panels. When the bulge reaches a certain size atoms start to emanate from it because the chemical potential here is enhanced relative to the vicinity. If this process dominates, the bulge will reverse and eventually the energy in the microcrack surface tends to be the same as under surface diffusion, as shown in the middle row of Figure 3. In addition, the driving force of the stress field and the electric field causes material to diffuse from the right side of the microcrack to the left. So the microcrack appears to migrate through the interconnect line. It can be seen that under different linewidths, the intragranular microcraks evolution tends to be two different trends. In other words, there must exist a critical linewidth $\hat{h}_c$. When $\hat{h} > \hat{h}_c$, the microcrack will evolve into a stable shape as it migrates along the interconnect line. In contrast, when $\hat{h} \leq \hat{h}_c$, the microcrack splits into two small parts.

Parts (d) and (e) of Figure 3 show that the splitting time of the microcrack decreases with a decrease in linewidth. Figure 4 shows the relationship of the splitting time $\hat{t}_f$ with the decrease of linewidth under different aspect ratios. It is obvious that the splitting time decreases as the linewidth decreases. This behavior indicates that the decrease in the linewidth accelerates the microcrack splitting process. Besides, it can be seen from the declining trend, when $\hat{h} < 25$ the influence of the size effect is distinct. When $\hat{h} > 25$, the variation of the curve is tardy, which means the effect of the size could almost be neglected. Compare the curves with different aspect ratios in Figure 3; it can be seen that the larger of the aspect ratio, the shorter time of the intragranular microcracks needed to spilt. That is, the increase of the aspect ratio is beneficial to microcrack splitting.

From this analysis, we conclude that the critical linewidth depends not only on the electric field but on the aspect ratio and the stress gradient. Figure 5, left, shows the critical linewidth of the microcrack splitting as a function of the electric field χ for four values of β when $\hat{p} = 15$. This figure indicates that $\hat{h}_c$ increases with the electric field. That is, the increase of the electric field is beneficial to the microcrack
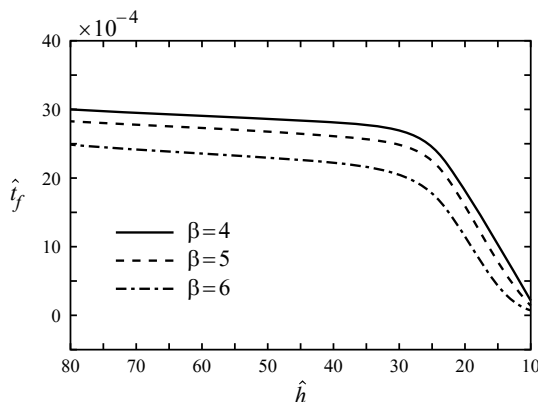
**Figure 4.** Dependence of $\hat{t}_f$ on $\hat{h}$ for $\chi = 0.6$, $\hat{p} = 29$.
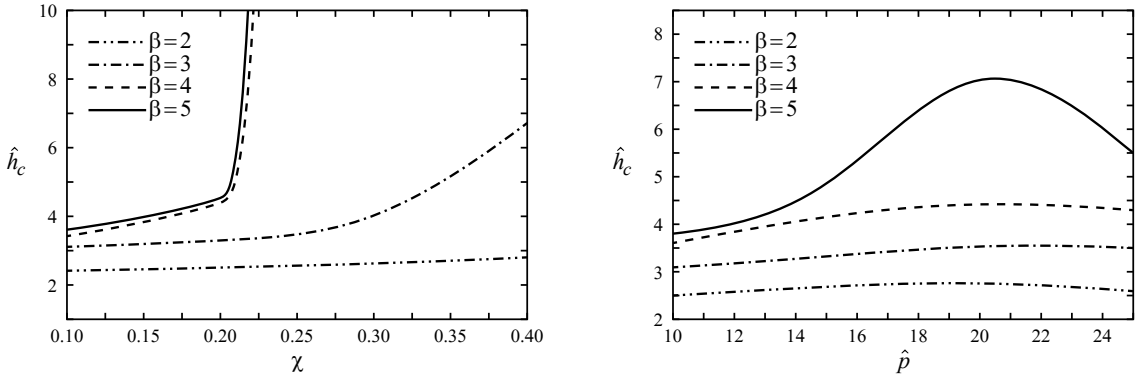
Figure 5. Left: dependence of $\hat{t}_c$ on χ for $\hat{p} = 15$.   Right: dependence of $\hat{t}_c$ on $\hat{p}$ for $\chi = 0.2$.

splitting. The critical linewidth increases as the increase of the aspect ratio for a given gradient stress and an electric field, which also manifests that the increase of the aspect ratio is also beneficial to the microcrack splitting. But its influence to the critical linewidth becomes very week when the aspect ratio exceeds a certain value. All microcracks for $\beta \geq 4$ split into two microcracks when $\chi > 0.22$.

Figure 5, right, shows the critical linewidth of the microcrack splitting as a function of the stress gradient under different aspect ratios for $\chi = 0.2$. For a given electric field and aspect ratio, the critical linewidth first increases and then decrease as the increase of the gradient stress field. When the stress gradient $\hat{p}$ is approximately equal to 20, the critical linewidth reaches its maximum. This feature is highlighted for the large microcrack.

Through a large number of numerical simulations, we also find that there exists a critical electric field χ_c for a given stress gradient $\hat{p}$, aspect ratio β and linewidth $\hat{h}$ and there exists a critical aspect ratio β_c for a given stress gradient $\hat{p}$, electric field χ and linewidth $\hat{p}$. There also exists a critical stress gradient $\hat{p}_c$ for a given electric field χ, aspect ratio β and linewidth $\hat{h}$. When $\chi < \chi_c$, $\beta < \beta_c$ or $\hat{p} < \hat{p}_c$, the microcrack will evolve into a stable shape as it migrates along the line. More interesting results are found that the microcrack splits into two small parts when $\chi > \chi_c$, $\beta > \beta_c$ or $\hat{p} > \hat{p}_c$.

Figure 6 shows the critical electric field χ_c as a function of the linewidth under different aspect ratios for $\hat{p} = 29$. The slope of these curves at any point represents the magnitude of the dependence. It can
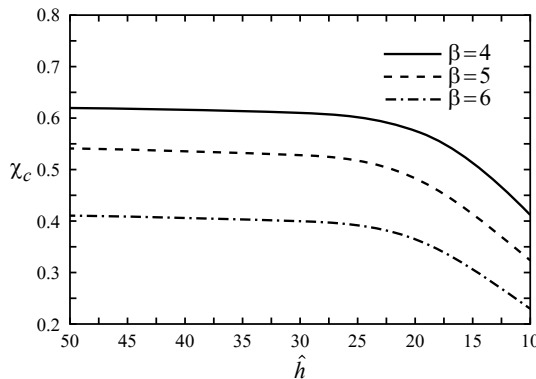
Figure 6. Dependence of χ_c on $\hat{h}$ for $\hat{p} = 29$.
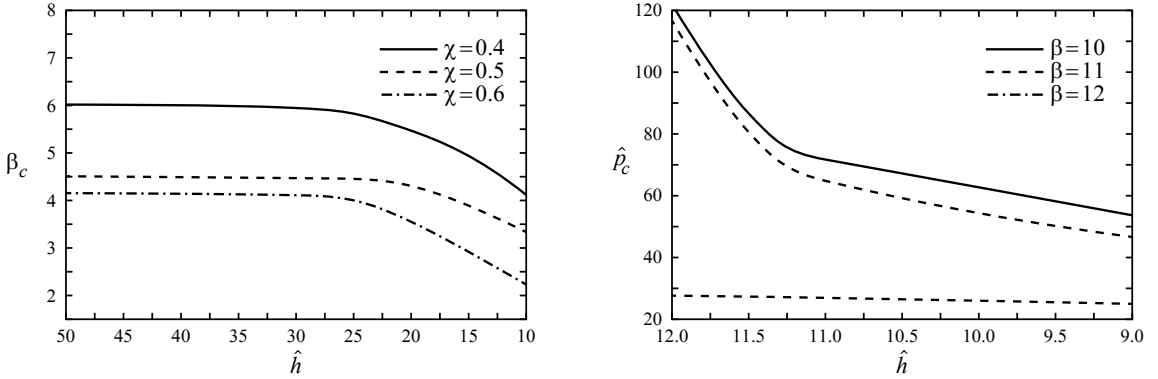
Figure 7. Left: dependence of β_c on $\hat{h}$ for $\hat{p} = 29$.   Right: Dependence of $\hat{p}_c$ on $\hat{h}$ for $\chi = 0.1$.

be seen from the variation tendency of the curve, the critical electric field decrease gradually with the decreases of linewidth, which demonstrates that the increasing current density accelerates the microcrack splitting. Moreover, we can find that the critical electric field dependence of the linewidth is relatively weakened when $\hat{h} \geq 25$. The results indicate that the influence of size effect could be ignored for this situation. Contrasting the three curves in the figure, it can be seen that the larger of the aspect ratio or the electric field of the microcrack, the easier for the microcrack to split. That is, the increase of aspect ratio and electric field are beneficial for the microcrack to split.

We turn to the variation in the critical aspect ratio β_c with $\hat{h}$ and χ. This is shown in Figure 7, left, as a function of the linewidth under different electric field for $\hat{p} = 29$. This figure indicates that the critical aspect ratio of the microcrack splitting decreases with the decrease of linewidth. That is to say, for a given electric field, the microcrack splitting will be much easy to occur with linewidth decreasing. Moreover, β_c decreases with an increase in the electric field, so such an increase is beneficial to microcrack splitting. It also can be seen from the the figure that the influence of size effect can be ignored when $\hat{h} \geq 25$.

Finally, Figure 7, right, shows the critical stress gradient $\hat{p}_c$ as a function of the linewidth under different aspect ratios for $\chi = 0.1$. We see that the critical stress gradient of the microcrack splitting decreases with the linewidth. In other words, for a given electric field and aspect ratio, microcrack splitting will occur more easily as the linewidth decreases. The critical stress gradient $\hat{p}_c$ also decreases with an increase in the aspect ratio. The critical stress gradient dependence on the linewidth is particularly noticeable for the larger microcrack when $\hat{h} > 11.3$.

5. Conclusion

In this paper, we derived the governing equation of the finite-element incorporating surface diffusion and evaporation/condensation induced both by stressmigration and electromigration. Then, the finite-element method was used to simulate the effect of interconnect linewidth on the evolution of microcracks under surface diffusion induced by the gradient stress field and the electric field. The main results obtained are summarized as follows:

(1) There must exist a critical linewidth $\hat{h}_c$. When $\hat{h} > \hat{h}_c$, the microcrack will evolve into a stable shape as it migrates along the interconnect line. When $\hat{h} \leq \hat{h}_c$, the microcrack splits into two small parts. The

splitting time decreases with the linewidth; that is, a decrease in the linewidth accelerates the microcrack splitting process. But the size effect could almost be neglected when $\hat{h} > 25$.

(2) The critical linewidth $\hat{h}_c$ depend not only on the electric field but also on the aspect ratio and the stress gradient. It increases with the electric field and the aspect ratio, while it first increases and then decreases as the stress gradient increases.

(3) There exists a critical electric field χ_c, a critical aspect ratio β_c and a critical stress gradient $\hat{p}_c$. When any of these variables are below those critical values, the microcrack evolves into a a stable shape as it migrates along the line, whereas when they exceed the critical values, the microcrack splits up.

(4) All three critical quantities decrease gradually with the decrease of linewidth. The influence of size effect on χ_c and β_c can be ignored when $\hat{h} \geq 25$, while the influence of size effect on $\hat{p}_c$ is very noticeable for the larger microcrack when $\hat{h} \geq 11.3$.

References

[Black 1969] J. R. Black, "Electromigration: a brief survey and some recent results", *IEEE. Trans. Electron Devices* **16**:4 (1969), 338–347.

[Blech 1998] I. A. Blech, "Diffusional back flows during electromigration", *Acta Mater.* **46**:11 (1998), 3717–3723.

[Blech and Herring 1976] I. A. Blech and C. Herring, "Stress generation by electromigration", *Appl. Phys. Lett.* **29**:3 (1976), 131–133.

[Bower and Craft 1998] A. F. Bower and D. Craft, "Analysis of failure mechanisms in the interconnect lines of microelectronic circuits", *Fatigue Fract. Eng. Mater. Struct.* **21**:5 (1998), 611–630.

[Bower and Freund 1993] A. F. Bower and L. B. Freund, "Analysis of stress-induced void growth mechanisms in passivated interconnect lines", *J. Appl. Phys.* **74**:6 (1993), 3855–3868.

[Bower and Shankar 2007] A. F. Bower and S. Shankar, "A finite element model of electromigration induced void nucleation, growth and evolution in interconnects", *Model. Simul. Mater. Sci. Eng.* **15**:8 (2007), 923–940.

[Cho and Thompson 1989] J. Cho and C. V. Thompson, "Grain size dependence of electromigration-induced failures in narrow interconnects", *Appl. Phys. Lett.* **54**:25 (1989), 2577–2579.

[Dalleau and Weide-Zaage 2001] D. Dalleau and K. Weide-Zaage, "Three-dimensional voids simulation in chip metallization structures: a contribution to reliability evaluation", *Microelectron. Reliab.* **41**:9-10 (2001), 1625–1630.

[Dong and Li 2009] X. Dong and Z. H. Li, "An analytical solution for motion of an elliptical void under gradient stress field", *Appl. Phys. Lett.* **94**:7 (2009), art. id. 071909.

[Dreyer and Varker 1992] M. L. Dreyer and C. J. Varker, "Electromigraton [sic] activation energy dependence on AlCu interconnect linewidth and microstructure", *Appl. Phys. Lett.* **60**:15 (1992), 1860–1862.

[Dwyer 2010] V. M. Dwyer, "An investigation of electromigration induced void nucleation time statistics in short copper interconnects", *J. Appl. Phys.* **107**:10 (2010), art. id. 103718.

[Dwyer 2011] V. M. Dwyer, "Analysis of critical-length data from electromigration failure studies", *Microelectron. Reliab.* **51**:9-11 (2011), 1568–1572.

[Fridline and Bower 1999] D. R. Fridline and A. F. Bower, "Influence of anisotropic surface diffusivity on electromigration induced void migration and evolution", *J. Appl. Phys.* **85**:6 (1999), 3168–3174.

[Fridline and Bower 2002] D. Fridline and A. Bower, "Numerical simulations of stress induced void evolution and growth in interconnects", *J. Appl. Phys.* **91**:4 (2002), 2380–2390.

[Giroux et al. 1995] F. Giroux, H. Roede, C. Gounelle, P. Mortini, and G. Ghibaudo, "Linewidth influence on electromigration tests at wafer level on TiN/AlCu/TiN/Ti metal lines", pp. 114–121 in *Conference on Microelectronic Manufacturing Yield, Reliability, and Failure Analysis* (Austin, TX, 1995), edited by G. Rao and M. Piccoli, Proc. SPIE **2635**, SPIE, Bellingham, WA, 1995.

[Gungor and Maroudas 1999] M. R. Gungor and D. Maroudas, "Nonhydrostatic stress effects on failure of passivated metallic thin films due to void surface electromigration", *Surf. Sci.* **432**:3 (1999), L604–L610.

[He and Huang 2014] D. He and P. Z. Huang, "A finite-element analysis of intragranular microcracks in metal interconnects due to surface diffusion induced by stress migration", *Comput. Mater. Sci.* **87** (2014), 65–71.

[He and Huang 2015] D. He and P. Z. Huang, "A finite-element analysis of in-grain microcracks caused by surface diffusion induced by electromigration", *Int. J. Solids Struct.* **62** (2015), 248–255.

[Herring 1999] C. Herring, "Surface tension as a motivation for sintering", pp. 33–69 in *Fundamental contributions to the continuum theory of evolving phase interfaces in solids*, edited by J. M. Ball et al., Springer, 1999.

[Huang and Sun 2004] P. Z. Huang and J. Sun, "A numerical analysis of intergranular penny-shaped microcrack shrinkage controlled by coupled surface and interface diffusion", *Metall. Mater. Trans. A* **35**:4 (2004), 1301–1309.

[Huang et al. 2003a] P. Z. Huang, Z. H. Li, J. Sun, and H. Gao, "Morphological healing evolution of intragranular penny-shaped microcracks by surface diffusion, I: Simulation", *Metall. Mater. Trans. A* **34**:2 (2003), 277–285.

[Huang et al. 2003b] P. Z. Huang, J. Sun, and Z. H. Li, "Axisymmetric finite-element simulation of grain growth behaviour", *Model. Simul. Mater. Sci. Eng.* **11**:1 (2003), 41–55.

[Huang et al. 2003c] P. Z. Huang, J. Sun, and Z. H. Li, "Evolution of penny-shaped microcracks by interface migration", *Int. J. Solids Struct.* **40**:8 (2003), 1959–1972.

[Huntington and Grone 1961] H. B. Huntington and A. R. Grone, "Current-induced marker motion in gold wires", *J. Phys. Chem. Solids* **20**:1-2 (1961), 76–87.

[Kraft and Arzt 1995] O. Kraft and E. Arzt, "Numerical simulation of electromigration-induced shape changes of voids in bamboo lines", *Appl. Phys. Lett.* **66**:16 (1995), 2063–2065.

[Kraft et al. 1993] O. Kraft, S. Bader, J. E. Sanchez, and E. Arzt, "Observation and modelling of electromigration-induced void growth in Al-based interconnects", *Mater. Res. Soc. Proc.* **309** (1993), 199–204.

[Krug and Dobbs 1994] J. Krug and H. T. Dobbs, "Current-induced faceting of crystal surfaces", *Phys. Rev. Lett.* **73**:14 (1994), 1947–1950.

[Li et al. 2010] Y. Li, Z. Li, X. Wang, and J. Sun, "Analytical solution for motion of an elliptical inclusion in gradient stress field", *J. Mech. Phys. Solids* **58**:7 (2010), 1001–1010.

[Lin et al. 2017] S.-K. Lin, Y.-C. Liu, S.-J. Chiu, Y.-T. Liu, and H.-Y. Lee, "The electromigration effect revisited: non-uniform local tensile stress-driven diffusion", *Sci. Rep.* **7** (2017), art. id. 3082.

[Liu and Yu 2006] Z. Liu and H.-H. Yu, "A numerical study on the effect of mobilities and initial profile in thin film morphology evolution", *Thin Solid Films* **513**:1-2 (2006), 391–398.

[Liu et al. 1998] Y. K. Liu, C. L. Cox, and R. J. Diefendorf, "Finite element analysis of the effects of geometry and microstructure on electromigration in confined metal lines", *J. Appl. Phys.* **83**:7 (1998), 3600–3608.

[Schimschak and Krug 1997] M. Schimschak and J. Krug, "Surface electromigration as a moving boundary value problem", *Phys. Rev. Lett.* **78**:2 (1997), 278–281.

[Sun and Suo 1997] B. Sun and Z. Suo, "A finite element method for simulating interface motion, II: Large shape change due to surface diffusion", *Acta Mater.* **45**:12 (1997), 4953–4962.

[Sun et al. 1994] B. Sun, Z. Suo, and A. G. Evans, "Emergence of cracks by mass transport in elastic crystals stressed at high temperatures", *J. Mech. Phys. Solids* **42**:11 (1994), 1653–1677.

[Sun et al. 1997] B. Sun, Z. Suo, and W. Yang, "A finite element method for simulating interface motion, I: Migration of phase and grain boundaries", *Acta Mater.* **45**:5 (1997), 1907–1915.

[Vairagar et al. 2004] A. V. Vairagar, S. G. Mhaisalkar, A. Krishnamoorthy, K. N. Tu, A. M. Gusak, M. A. Meyer, and E. Zschech, "In situ observation of electromigration-induced void migration in dual-damascene Cu interconnect structures", *Appl. Phys. Lett.* **85**:13 (2004), 2502–2504.

[Vanstreels et al. 2014] K. Vanstreels, P. Czarnecki, T. Kirimura, Y. K. Siew, I. D. Wolf, J. Bömmels, Z. Tőkei, and K. Croes, "In-situ scanning electron microscope observation of electromigration-induced void growth in 30 nm 1/2 pitch Cu interconnect structures", *J. Appl. Phys.* **115**:7 (2014), art. id. 074305.

[Wang and Yao 2017a] Y. Wang and Y. Yao, "A theoretical analysis of the electromigration-induced void morphological evolution under high current density", *Acta Mech. Sinica* **33**:5 (2017), 868–878.

[Wang and Yao 2017b] Y. Wang and Y. Yao, "A theoretical analysis to current exponent variation regularity and electromigration-induced failure", *J. Appl. Phys.* **121**:6 (2017), art. id. 065701.

[Wang et al. 2006] H. Wang, Z. H. Li, and J. Sun, "Effects of stress and temperature gradients on the evolution of void in metal interconnects driven by electric current and mechanical stress", *Model. Simul. Mater. Sci. Eng.* **14**:4 (2006), 607–615.

[Xia et al. 1997] L. Xia, A. F. Bower, Z. Suo, and C. F. Shih, "A finite element analysis of the motion and evolution of voids due to strain and electromigration induced surface diffusion", *J. Mech. Phys. Solids* **45**:9 (1997), 1473–1493.

[Yao et al. 2009] Y. Yao, L. M. Keer, and M. E. Fine, "Electromigration effect on pancake type void propagation near the interface of bulk solder and intermetallic compound", *J. Appl. Phys.* **105**:6 (2009), art. id. 063710.

[Zhang et al. 1998] Y. W. Zhang, A. F. Bower, L. Xia, and C. F. Shih, "Three dimensional finite element analysis of the evolution of voids and thin films by strain and electromigration induced surface diffusion", *J. Mech. Phys. Solids* **47**:1 (1998), 173–199.

[Zhang et al. 2010] L. Zhang, J. P. Zhou, J. Im, P. S. Ho, O. Aubel, C. Hennesthal, and E. Zschech, "Effects of cap layer and grain structure on electromigration reliability of Cu/low-k interconnects for 45 nm technology node", pp. 581–585 in *2010 IEEE International Reliability Physics Symposium* (Anaheim, CA, 2010), IEEE, Piscataway, NJ, 2010.

[Zschech et al. 2010] E. Zschech, R. Hübner, O. Aubel, and P. S. Ho, "EM and SM induced degradation dynamics in copper interconnects studied using electron microscopy and X-ray microscopy", pp. 574–580 in *IEEE International Reliability Physics Symposium* (Anaheim, CA, 2010), IEEE, Piscataway, NJ, 2010.

LINYONG ZHOU: zhouly@nuaa.edu.cn
*State Key Laboratory of Mechanics and Control of Mechanical Structures, Nanjing University of Aeronautics and Astronautics,
29 Yudao Street, Nanjing, 210016, China*

PEIZHEN HUANG: pzhuang@nuaa.edu.cn
*State Key Laboratory of Mechanics and Control of Mechanical Structures, Nanjing University of Aeronautics and Astronautics,
29 Yudao Street, Nanjing, 210016, China*

QIANG CHENG: qcheng@nuaa.edu.cn
*State Key Laboratory of Mechanics and Control of Mechanical Structures, Nanjing University of Aeronautics and Astronautics,
29 Yudao Street, Nanjing, 210016, China*

JOURNAL OF MECHANICS OF MATERIALS AND STRUCTURES

msp.org/jomms

Founded by Charles R. Steele and Marie-Louise Steele

PUBLISHED BY

mathematical sciences publishers

nonprofit scientific publishing

http://msp.org/

Journal of Mechanics of Materials and Structures

Volume 13, No. 3   May 2018